HHS Public Access

Author manuscript

Nature. Author manuscript; available in PMC 2012 November 17.

Published in final edited form as:

Nature. 2012 May 17; 485(7398): 391–394. doi:10.1038/nature10998.

A PPARγ-FGF1 axis is required for adaptive adipose remodelling and metabolic homeostasis

Johan W. Jonker[1,†,*], **Jae Myoung Suh**[1,*], **Annette R. Atkins**[1], **Maryam Ahmadian**[1], **Pingping Li**[3], **Jamie Whyte**[1], **Mingxiao He**[1], **Henry Juguilon**[1], **Yun-Qiang Yin**[1], **Colin T. Phillips**[1], **Ruth T. Yu**[1], **Jerrold M. Olefsky**[3], **Robert R. Henry**[3,4], **Michael Downes**[1], and **Ronald M. Evans**[1,2]

[1]Gene Expression Laboratory, Salk Institute for Biological Studies, 10010 N Torrey Pines Rd, La Jolla, California 92037

[2]Howard Hughes Medical Institute, Salk Institute for Biological Studies, 10010 N Torrey Pines Rd, La Jolla, California 92037

[3]Department of Medicine, Division of Endocrinology and Metabolism, University of California at San Diego, La Jolla, CA 92093

[4]Veterans Affairs San Diego Healthcare System, San Diego

Keywords

FGF1; PPARγ; Thiazolidinedione; adipose remodelling; insulin resistance

While feast and famine cycles illustrate that adipose tissue remodelling in response to fluctuations in nutrient availability is essential for maintaining metabolic homeostasis, the underlying mechanisms remain poorly understood[1,2]. Here, we identify fibroblast growth factor (FGF) 1 as a critical transducer in this process and link its regulation to the nuclear receptor (NR) PPARγ, the adipocyte master regulator and target of the thiazolidinedione (TZD) class of insulin sensitizing drugs[3–5]. FGF1 is the prototype of the 22 member FGF family of proteins and has been implicated in a range of physiological processes including development, wound healing and cardiovascular changes[6]. Surprisingly, FGF1 knockout

Address correspondence to: Ronald M. Evans, Gene Expression Laboratory & Howard Hughes Medical Institute, Salk Institute for Biological Studies, 10010 N Torrey Pines Rd, La Jolla, California 92037. Phone: 858-453-4100, fax: 858-455-1349, evans@salk.edu. Michael Downes, Gene Expression Laboratory, Salk Institute for Biological Studies, 10010 N Torrey Pines Rd, La Jolla, California 92037. Phone: 858-453-4100, fax: 858-455-1349, downes@salk.edu.

[†]Present address: Center for Liver, Digestive and Metabolic Diseases, Department of Pediatrics, University Medical Center Groningen, University of Groningen, Groningen, The Netherlands.

[*]These authors contributed equally to this work.

Author contributions

J.W.J, J.M.S, M.D. and R.M.E. designed and supervised the research. J.W.J., J.M.S., A.R.A., M.A., P.L., M.H., J.W., H.J., Y-Q.Y. and C.T.P. performed research. R.R.H. provided samples and analysed results. J.W.J., J.M.S., R.T.Y., J.M.O., M.D. and R.M.E. analysed data. J.W.J, J.M.S., A.R.A., M.A., M.D. and R.M.E. wrote the manuscript.

Author Information

Microarray data sets have been deposited in the NCBI Gene Expression Omnibus, accession number GSE31692. Reprints and permissions information is available at www.nature.com/reprints.

The authors declare no competing financial interests.

mice display no significant phenotype under standard laboratory conditions[7–9]. We show that FGF1 is highly induced in adipose tissue in response to high-fat diet (HFD) and that mice lacking FGF1 develop an aggressive diabetic phenotype coupled to aberrant adipose expansion when challenged with HFD. Further analysis of adipose depots in FGF1 deficient mice revealed multiple histopathologies in the vasculature network, an accentuated inflammatory response and aberrant adipocyte size distribution. Upon HFD withdrawal, this inflamed adipose tissue fails to properly resolve resulting in ectopic expression of pancreatic lipases and extensive fat necrosis. Mechanistically, we show that adipose induction of FGF1 in the fed state is regulated by PPARγ acting through an evolutionarily conserved promoter proximal PPAR response element within the *FGF1* gene. This work describes the first phenotype of the FGF1 knockout mouse and establishes the PPARγ-FGF1 axis as critical for maintaining metabolic homeostasis and insulin sensitization.

As part of a directed screen to identify genes that respond to dietary cues in metabolic tissues (muscle, liver, brown adipose (BAT) and white adipose tissue (WAT)), we observed that FGF1 is selectively induced in visceral (*i.e.* gonadal) WAT (gWAT) in response to a high-fat diet (HFD), pointing to a possible metabolic function (Fig. 1a, Supplementary Fig. 1a, b). Subfractionation of adipose depots revealed that FGF1 was expressed in the adipocyte fraction but not in the stromal vascular fraction (SVF) of gWAT, and to a lesser extent in the adipocyte fraction of subcutaneous (*i.e.* inguinal) WAT (iWAT) (Fig. 1b). Given that *FGF1* gene transcription is directed by at least three distinct promoters that are conserved across mammals[10] (Fig. 1c), we examined the tissue-specific expression patterns of each isoform. While *FGF1A* and *FGF1B* were both expressed in gWAT (as well as other tissues) of mice fed a standard chow diet (Fig. 1d–f), only *FGF1A* showed a striking and progressive 20-fold induction between fasted, fed, and HFD exposure (Fig. 1g, h). While no metabolic role has been attributed to FGF1, these results prompted us to reconsider this possibility. Consistent with previous reports, no metabolic or histological abnormalities, or major gene expression changes were observed in $FGF1^{-/-}$ mice fed a standard chow diet[7] (Supplementary Fig. 1c, 2, Supplementary Table 3). Similarly, when placed on a HFD, $FGF1^{-/-}$ and wild-type cohorts showed equivalent changes in weight (monitored for 24 weeks), serum adipokines, cytokines (leptin, resistin, IL-6, TNFα, tPAI-1, total and HMW adiponectin) as well as serum lipids (cholesterol, free fatty acids, and triglycerides) (Fig. 1i, Supplementary Tables 1 and 2). However, $FGF1^{-/-}$ mice developed an exaggerated diabetic phenotype, with increased levels of fasting glucose and insulin (Fig. 2a), accompanied by severe insulin resistance (Fig. 2b, c) and markedly enhanced serum MCP-1/CCL2 (48.0 ± 3.4 compared to 59.0 ± 3.4 pg/ml, $P < 0.01$, in wild-type and $FGF1^{-/-}$ mice, respectively), a marker of adipose macrophage infiltration and a causative factor for peripheral insulin resistance[11,12]. To further investigate the role of FGF1 in insulin sensitivity, we performed hyperinsulinemic-euglycemic clamp studies. The steady-state glucose infusion rate (GIR) during the clamp was about 40% lower in HFD-fed $FGF1^{-/-}$ mice, reflecting decreased insulin responsiveness, and was accompanied by reductions in whole body and insulin-stimulated glucose disposal rates (GDR and IS-GDR) indicating pronounced peripheral insulin resistance (Fig. 2d–f). The ability of insulin to suppress hepatic glucose production (HGP) was also significantly compromised in HFD-fed $FGF1^{-/-}$mice, revealing hepatic insulin resistance as well (Fig. 2g). Although HFD-fed $FGF1^{-/-}$ mice had enlarged steatotic

livers relative to wild-type controls (Fig. 2h, i), liver function (based on serum ALT levels) and pancreatic function (based on islet histology and insulin secretion) appeared normal (Supplementary Fig. 3, 4). On the other hand, gWAT in *FGF1*$^{-/-}$mice failed to expand after HFD and exhibited pronounced structural abnormalities as evidenced by hematoxylin and eosin staining (Fig. 2j, k, Supplementary Fig. 5). As expected with higher circulating levels of MCP-1, we observed a dramatic increase in macrophage infiltration, indicating a highly inflamed gWAT (Fig. 3a). Notably, no defects were observed in iWAT (data not shown). This differential sensitivity of WAT depots to HFD stress is consistent with the known association of the visceral WAT with obesity-related pathologies including insulin resistance[13].

To explore the possibility that the metabolic dysregulation observed in *FGF1*$^{-/-}$ mice on a HFD was associated with defects in gWAT, we performed detailed histological and molecular analyses of this tissue. Histochemistry with Masson's trichrome stain of gWAT from the HFD-fed *FGF1*$^{-/-}$ mice revealed increased collagen deposition (blue staining) and a marked heterogeneity in adipocyte size (Fig. 3b). Quantification of adipocyte cross-sectional areas showed increases in the numbers of both small and large adipocytes in *FGF1*$^{-/-}$ mice relative to wild-type (Fig. 3c). Next we examined the functional architecture of the adipose vasculature by intravenous injection of fluorescent microbeads. Epifluorescence microscopy of tissue sections from fluorescent bead-perfused mice revealed decreased vascular density specifically in gWAT (Fig. 3d) but not in BAT or iWAT of HFD-fed *FGF1*$^{-/-}$ mice (Supplementary Fig. 6). Microarray analyses identified multiple transcriptional changes induced by HFD in *FGF1*$^{-/-}$ gWAT that were consistent with the observed phenotypes. The obesity and insulin resistance markers RBP4 and CCL11 were upregulated by HFD, as was the angiogenic factor VEGF. Interestingly, expression of PPARγ was also induced by HFD in *FGF1*$^{-/-}$ gWAT, as were known PPARγ target genes (e.g. perilipin, DGAT1, DGAT2) (Supplementary Table 3). However, the most dramatic inductions of gene expression were seen in multiple fat necrosis-associated pancreatic lipases and the tissue remodelling factor elastase 1, which were confirmed by qPCR (Fig. 3e, Supplementary Table 3)[14–16]. Taken together, the observed histopathological and molecular changes in *FGF1*$^{-/-}$ gWAT suggested a failure to execute the appropriate adipose remodelling program in response to HFD stress. As adipose tissue needs to dynamically expand and contract with fluctuations in nutrient availability, we postulated that FGF1 would also play a role in its contraction capacity upon withdrawal from HFD. To test this, we re-adapted HFD-fed wild-type and *FGF1*$^{-/-}$ mice to 6 weeks of chow feeding. Gross examination of HFD-to-chow converted (HCC) mice revealed features consistent with maladaptation resulting in disfigurement and discoloration of gWAT from *FGF1*$^{-/-}$ mice compared to control wild-type mice (Fig. 3f). Histological examination of the HCC *FGF1*$^{-/-}$gWAT showed profound degeneration of adipose architecture and integrity of far greater severity than the HCC wild-type gWAT (Fig. 3g). Indeed, HCC *FGF1*$^{-/-}$ mice frequently presented with what appeared to be fragments of dissociated fat tissue within the peritoneal cavity, which upon histological analysis were consistent with a fat necrosis pathology (Fig. 3h). The observations from the HFD and HCC regimens demonstrate a dynamic requirement for FGF1 in both adipose tissue expansion and contraction. Together our findings show that when challenged with a HFD or HCC, *FGF1*$^{-/-}$ mice are unable to

remodel visceral adipose tissue in response to dietary changes. This suggests that defects in adipose plasticity, attributable to the loss of FGF1, are causally linked with a series of peripheral pathologies including hepatic steatosis and systemic insulin resistance. These results establish FGF1 as a transducer of adipose remodelling in response to nutrient fluctuations, and identify an indispensible role for FGF1 in defending the body against metabolic disease.

As PPARγ expression was induced in *FGF1*$^{-/-}$ gWAT by HFD, and HFD elevates the levels of circulating PPAR ligands[17,18], we postulated that the HFD-induction of *FGF1A* may be regulated by a PPAR family member. Luciferase reporter assays indeed revealed a robust induction of the human *FGF1A* promoter by the PPARs, of which PPARγ was the most potent (Fig. 4a). Furthermore, in this system the PPAR induction of FGF1 appears isoform specific, as PPARs did not induce *FGF1B*, the other *FGF1* isoform expressed in WAT (Fig. 4b). Examination of the promoter region of *FGF1A* revealed a highly conserved (98% conservation) region ~100 bp proximal to the transcription start site (TSS) (Supplementary Fig. 7a) containing a conserved putative PPAR response element (PPRE) at −60 bp relative to the TSS (Fig. 4c). Inactivation of this PPRE using site directed mutagenesis resulted in a complete loss of its response to PPARγ (Fig. 4c, d: compare human vs ΔPPRE). To examine the functional conservation of FGF1 regulation by PPARγ, we assayed the native human and mouse *FGF1A* promoters along with reporter constructs containing orthologous PPREs (rat, horse, opossum) introduced into the human *FGF1A* promoter. PPARγ activation was observed for all promoters except for the more distantly related opossum PPRE (Fig. 4d). Chromatin immuno-precipitation (ChIP) experiments confirmed that PPARγ does indeed bind to the identified PPRE in 3T3-L1 adipocytes (Fig. 4e, Supplementary Fig. 7b). Data mining of a published genome-wide PPARγ ChIP-Seq study indicates that the PPARγ-*FGF1A* interaction may be specific to WAT, as PPARγ binding was seen in 3T3-L1 cells, but not in macrophages[19]. Together, these findings show that the adipocyte PPARγ-FGF1 axis is functionally conserved in a wide range of mammals.

To confirm the physiological relevance of the PPARγ induction of FGF1, we determined the expression of the *FGF1A* transcript in mice in response to the potent and specific PPARγ ligand rosiglitazone (TZD). We found that oral administration of rosiglitazone (5 mg/kg for 3 days) significantly increased the mRNA levels of *FGF1A* in gWAT, in fed but not fasted states (Fig. 4f). *FGF1B* and *FGF1D* expression was unchanged by rosiglitazone in gWAT and liver (Fig 4g; Supplementary Fig. 8) whereas *FGF1A* and *FGF1D* were undetectable in liver and gWAT, respectively (data not shown). Further, adipocyte-specific PPARγ knockout mice[20] displayed decreased levels of FGF1 in the adipocyte fraction, without compensatory changes in the closely related FGF2, which was only detected in the SVF (Fig. 4h).

In conclusion, we have discovered an unexpected metabolic role for FGF1 as a critical transducer of PPARγ signalling that mediates the proper coupling of nutrient storage to adaptive remodelling of adipose tissue. We found that HFD results in potent and selective induction of FGF1 in adipose tissue and that its transcription is controlled by PPARγ and its insulin sensitizing ligands. Loss of FGF1 leads to systemic metabolic dysfunction and insulin resistance, revealing an indispensable role for FGF1 in metabolic homeostasis (Fig.

4i). Importantly, we show that *FGF1*$^{-/-}$ mice are unable to both properly expand and contract their adipose tissue in response to dietary changes, revealing the dynamic requirement of FGF1 for adipose tissue remodelling. The capacity of adipose tissue to remodel is crucial for accommodating changes in energy availability in fasted and fed states but is not unlimited, and can become perturbed in obesity and related pathologies. Previous reports have shown that FGF1 can signal through FGFRs to pre-adipocytes[21–23]. Recently, several endocrine FGF family members (FGF15/19, 21) have been linked to metabolic homeostasis through NR regulation[24–26]. We now expand this NR-FGF interface to include the paracrine FGF1. Our discovery of the PPARγ-FGF1 axis leads us to consider the therapeutic potential of FGF1 in potentially mediating insulin sensitization without provoking the full range of adverse events associated with PPARγ activation.

Methods summary

FGF1$^{-/-}$ mice and age and sex-matched wild-type controls (>99% C57BL/6 genetic background) received a standard diet or high fat (60%) diet (F3282, Bio-Serv) and water *ad libitum*. For the HFD-to-chow conversion diet regimen (HCC), mice were fed HFD starting from 6 weeks of age. After 9 months of HFD, the diet was converted back to standard laboratory chow for 6 weeks. Glucose tolerance tests (GTT) and Insulin tolerance tests (ITT) were conducted after overnight and 5 hour fasting, respectively. Glucose (1g/kg i.p.) or insulin (0.5 U insulin/kg i.p.) was injected and blood glucose monitored. Serum analyses were performed on blood collected by tail bleeding either in the *ad libitum* fed state or following overnight fasting. Free fatty acids, triglycerides, cholesterol and ALT were measured using commercial enzymatic colorimetric kits. Serum insulin levels and total and high-molecular weight (HMW) adiponectin levels were measured by ELISAs using commercial kits. Plasma adipokine levels were measured using a Milliplex™ MAP kit. Histological and immunohistochemical analyses were performed on sections of fixed tissues according to standard procedures.

Vasculature was visualized by tail vein injection of fluorescent microbeads (0.1 μm FluoSpheres®, Molecular Probes). Subsequently, mice were anesthetized and perfused through the heart with additional fluorescent microbeads. Tissues were dissected, embedded and 10 μm frozen sections analyzed for blood vessel density using fluorescence microscopy.

Luciferase reporter assays were performed in CV-1 cells treated overnight with or without ligands (PPARα, 1 μM WY14643; PPARγ, 1 μM Rosiglitazone (TZD); PPARδ, 100 nM GW1516). Site-directed mutagenesis of the PPRE in the human promoter was performed using a QuikChange II kit.

Chromatin immunoprecipitation assays were performed on differentiated 3T3-L1 cells. Sheared chromatin generated from cross-linked cell pellets by sonication was incubated with PPARγ antibody or control rabbit IgG, and precipitated with pre-blocked protein A-agarose beads.

Methods

Animals

FGF1$^{-/-}$ mice[7] and age and sex-matched wild-type controls (>99% C57BL/6 genetic background) received a standard chow diet (MI laboratory rodent diet 5001, Harlan Teklad) or high fat (60%) diet (F3282, Bio-Serv) and water *ad libitum*. PPARγ$^{fl/fl}$ mice were crossed with *aP2-Cre* mice to generate *aP2-Cre; PPARγ*$^{fl/fl}$ mutant mice as previously described[20] and received standard chow up to analysis at five months of age. All mice used for studies were male unless otherwise noted.

Reporter assays

Luciferase reporter assays were performed in CV-1 cells treated overnight with or without ligands (PPARα, 1 μM WY14643; PPARγ, 1 μM Rosiglitazone (TZD); PPARδ, 100 nM GW1516). Site directed mutagenesis of the PPRE in the human promoter was performed using a QuikChange II kit (Stratagene, La Jolla, CA).

Western analysis

Total cell lysates prepared in 50 mM Tris-HCl, pH 8.0, 150 mM NaCl, 1% Triton-X100, 0.1% SDS, 2 mM sodium azide and protease inhibitor cocktail (Complete, Roche), were resolved by SDS-PAGE and probed using primary antibodies to FGF1, FGF2 (Santa Cruz) and ERK1/2 (Cell Signaling Technology).

Serum analysis

Blood was collected by tail bleeding either in the *ad libitum* fed state or following overnight fasting. Free fatty acids (Wako), triglycerides (Thermo), cholesterol (Thermo) and ALT (Thermo) were measured using enzymatic colorimetric methods. Serum insulin levels (Ultra Sensitive Insulin, Crystal Chem) and total and high-molecular weight (HMW) adiponectin levels (ALPCO) were measured by ELISAs. Plasma adipokine levels were measured using a Milliplex™ MAP kit (Millipore).

Histological analysis and immunohistochemistry

4 μm sections of fixed tissues were stained with hematoxylin and eosin according to standard procedures. For immunohistochemistry, tissues were deparaffinized in xylene and rehydrated. Slides were incubated with 5% normal donkey serum for 30 min, followed by overnight incubation with primary and secondary antibodies (F4/80, Abcam, 1:100).

Adipocyte Size Analysis

Adipocyte cross-sectional area was determined from photomicrographs of gonadal, mesenteric, and inguinal fat pads using ImageJ[27].

Adipose tissue fractionation

Adipose tissues were excised and finely minced with a razor blade. Minced tissue was digested in adipocyte isolation buffer (100mM HEPES pH7.4, 120mM NaCl, 50mM KCl, 5mM glucose, 1mM CaCl2, 1.5% BSA) containing 1mg/ml collagenase at 37°C with

constant slow shaking (~120rpm) for 2 hours. During the digestion period, the suspension was gently mixed several times. The suspension was then passed through a 200μm mesh and 100μm successively. The flowthrough was allowed to stand for 15 min to separate the floating adipocyte fraction and infranatant containing the stromal vascular fraction. The infranatant was removed and saved while minimally disturbing the floating adipocyte fraction. Both fractions were centrifuged at 500xg for 10 minutes and further washed twice in DMEM/Ham's F-12 media before further manipulation.

Metabolic studies

Glucose tolerance tests (GTT) and Insulin tolerance tests (ITT) were conducted after o/n and 5 hour fasting, respectively[28,29]. Glucose (1g/kg i.p.) or insulin (0.5 U insulin/kg i.p.) was injected and blood glucose monitored using a OneTouch Ultra glucometer (Lifescan Inc).

Hyperinsulinemic-euglycemic clamp

Mouse clamps were performed as previously described[27,28]. Briefly, mice implanted with dual jugular catheters 3 days prior were fasted for 6 hr, then equilibrated with tracer (5.0 μCi/h, 0.12 ml/h [3-3H]D-glucose, NEN Life Science Products) for 90 min. A basal blood sample was then drawn via tail vein to calculate basal glucose uptake. The insulin (8 mU/kg/min at 2 μl/min, Novo Nordisk) plus tracer (5.0 μCi/h) and glucose (50% dextrose at variable rate, Abbott) infusions were initiated simultaneously, with the glucose flow rate adjusted to reach a steady state blood glucose concentration (~120 min). Steady state was confirmed by stable plasma tracer counts during the final 30 min of clamp. Blood was taken at 110 and 120 minutes for the determination of tracer-specific activity. At steady state, the rate of glucose disappearance or the total GDR is equal to the sum of the rate of endogenous or HGP plus the exogenous GIR. The IS-GDR is equal to the total GDR minus the basal glucose turnover rate.

Gene Expression Analysis

Total RNA was isolated from mouse tissue and cells using TRIzol reagent (Invitrogen). cDNA was synthesized from 1 μg of DNAse-treated total RNA using SuperScript II reverse transcriptase (Invitrogen). mRNA levels were quantified by QPCR with SYBR Green (Invitrogen). Samples were run in technical triplicates and relative mRNA levels were calculated by using the standard curve methodology and normalized against *36B4* mRNA levels in the same samples.

Microarrays

500 ng of total RNA extracted from gWAT (24 wk old wild-type and *FGF1*$^{-/-}$ mice on chow or HFD) using Trizol reagent (Invitrogen) was reverse transcribed into cRNA and biotin-UTP labeled using the Illumina TotalPrep RNA Amplification Kit (Ambion). cRNA was hybridized to the Illumina mouseRefseq-8v2 Expression BeadChip using standard protocols (Illumina). Image data was converted into unnormalized Sample Probe Profiles using the Illumina BeadStudio software and analyzed by VAMPIRE. Stable variance models were constructed for each experimental conditions (n=2). Differentially expressed probes were identified (unpaired VAMPIRE significance test with a 2-sided, Bonferroni-corrected

threshold of $\alpha_{Bonf} = 0.05$) and the significance of apparent differences between 2 experimental conditions determined. Lists of altered genes were mapped to pathways (VAMPIRE tool Goby) to determine KEGG categories overrepresented (Bonferroni error threshold of $\alpha_{Bonf} = 0.05$).

Chromatin immunoprecipitation assay (ChIP)

Adipocytes differentiated from 3T3-L1 cells[29] (ATCC) were sequentially cross-linked with 2mM Disuccinimidyl glutarate (30 min at RT) and 1% formaldehyde (10 min at RT). Crosslinking was quenched with glycine, and the washed cell pellet frozen at −80°. Cell pellets were lysed and centrifuged at 12,000 × g for 1min at 4°C. Sheared chromatin generated from cell pellets by sonication was incubated with PPARγ antibody (2μg sc-7196, overnight at 4°C) or control rabbit IgG (sc-2027, Santa Cruz Biotechnologies). The immuno-complexes were precipitated with 20μl pre-blocked protein A-agarose beads (1h at 4°C) and washed extensively[30].

Input DNA isolation, DNA de-crosslinking, purification and analysis

Sheared input chromatin was ethanol precipitated and Chelex 100 (100μl of 10% slurry, Bio-Rad) added to both input DNA and washed ChIP samples. Samples were vortexed, boiled for 10min and then centrifuged (12,000 × g for 1min). Samples were treated with proteinase K (1μl of 20mg/ml, 55°C for 30min), heat deactivated, and the DNA purified (Qiagen MinElute PCR Purification Kit) prior to qPCR analysis using the following primers:

FGF1 Fw 5′-AGAGTAGGGCACAGACACAGC-3′

FGF1 Rev 5′-TGGATTAGACACGCAGGCTA-3′

aP2 Fw 5′-ATTTGCCTTCTTACTGGATCAGAGTT-3′

aP2 Rev 5′-TTGGGCTGTGACACTTCCAC-3′

Angpl4 Fw 5′-CCAGCCAGGGAAAGTAGGAGA-3′

Angpl4 Rev 5′-CAGAAAGTGCCTGCATGCC-3′

36b4 Fw 5′-GCCAATAGACGCGCATGTTT-3′

36b4 Rev 5′-TGGTTCCATCGACTGTCCTG-3′

Fluorescent microbead perfusion for vasculature studies

Mice were tail vein injected with 150 μl of PBS fluorescent microbeads (0.1 μm red fluorescent microbeads, Invitrogen), anesthetized 5 minutes later, then perfused through the heart with 6 ml of 1:10 PBS dilution of fluorescent microbeads. Tissues were then dissected and embedded in Tissue-Tek®OCT compound (Sakura) and 10μm frozen sections were mounted in Vectashield® medium (Vector Laboratories) for analysis of blood vessel density using fluorescence microscopy[31].

Statistical analysis

All values are given as means ± standard errors. The two-tailed unpaired Student's *t*-test was used to assess the significance of difference between two sets of data. Differences were considered to be statistically significant when $P < 0.05$.

Supplementary Material

Refer to Web version on PubMed Central for supplementary material.

Acknowledgments

We thank Jackie Alvarez, Samantha Kaufman, N. Henriette Uhlenhaut, Mojibade Hassan, and Elliot Williams for technical assistance, and Lita Ong and Sally Ganley for administrative assistance. R.M.E. is an Investigator of the Howard Hughes Medical Institute at the Salk Institute and March of Dimes Chair in Molecular and Developmental Biology. This work was supported by National Institutes of Health Grants (DK062434, DK057978, DK090962, DK063491 and HL105278), the Helmsley Charitable Trust, and the Howard Hughes Medical Institute. J.W.J. is supported by the Human Frontier Science Program (HFSP), the Netherlands Organization for Scientific Research (NWO) and an EU Marie Curie Reintegration Grant (IRG-277169). M.A. is supported by an F32 Ruth L. Kirschstein National Research Service Award (NIDDK).

References

1. Lee MJ, Wu Y, Fried SK. Adipose tissue remodeling in pathophysiology of obesity. Curr Opin Clin Nutr Metab Care. 2010; 13:371–6. [PubMed: 20531178]
2. Sun K, Kusminski CM, Scherer PE. Adipose tissue remodeling and obesity. J Clin Invest. 2011; 121:2094–101. [PubMed: 21633177]
3. Forman BM, et al. 15-Deoxy-$\Delta^{12,14}$-Prostaglandin J_2 is a ligand for the adipocyte determination factor PPARγ. Cell. 1995; 83:803–812. [PubMed: 8521497]
4. Barak Y, et al. PPAR gamma is required for placental, cardiac, and adipose tissue development. Mol Cell. 1999; 4:585–595. [PubMed: 10549290]
5. Tontonoz P, Spiegelman BM. Fat and beyond: the diverse biology of PPARgamma. Annu Rev Biochem. 2008; 77:289–312. [PubMed: 18518822]
6. Itoh N, Ornitz DM. Functional evolutionary history of the mouse Fgf gene family. Dev Dyn. 2008; 237:18–27. [PubMed: 18058912]
7. Miller DL, Ortega S, Bashayan O, Basch R, Basilico C. Compensation by Fibroblast Growth Factor 1 (FGF1) does not account for the mild phenotypic defects observed in FGF2 null mice. Mol Cell Biol. 2000; 20:2260–2268. [PubMed: 10688672]
8. Beenken A, Mohammadi M. The FGF family: biology, pathophysiology and therapy. Nat Rev Drug Discov. 2009; 8:235–253. [PubMed: 19247306]
9. Itoh N, Ornitz DM. Fibroblast growth factors: from molecular evolution to roles in development, metabolism and disease. J Biochem. 2011; 149:121–30. [PubMed: 20940169]
10. Myers RL, Payson RA, Chotani MA, Deaven LL, Chiu IM. Gene structure and differential expression of acidic fibroblast growth factor mRNA: identification and distribution of four different transcripts. Oncogene. 1993; 8:341–349. [PubMed: 7678925]
11. Kanda H, et al. MCP-1 contributes to macrophage infiltration into adipose tissue, insulin resistance, and hepatic steatosis in obesity. J Clin Invest. 2006; 116:1494–1505. [PubMed: 16691291]
12. Kamei N, et al. Overexpression of monocyte chemoattractant protein-1 in adipose tissues causes macrophage recruitment and insulin resistance. J Biol Chem. 2006; 281:26602–14. [PubMed: 16809344]
13. Gesta S, Tseng YH, Kahn CR. Developmental origin of fat: tracking obesity to its source. Cell. 2007; 131:242–256. [PubMed: 17956727]

14. Schmitz-Moormann P, von Wedel R, Agricola B, Himmelmann GW. Studies of lipase-induced fat necrosis in rats. Pathol Res Pract. 1978; 163:93–108. [PubMed: 569296]
15. Lee PC, Nakashima Y, Appert HE, Howard JM. Lipase and colipase in canine pancreatic juice as etiologic factors in fat necrosis. Surg Gynecol Obstet. 1979; 148:39–44. [PubMed: 758695]
16. Chua F, Laurent GJ. Neutrophil elastase: mediator of extracellular matrix destruction and accumulation. Proc Am Thorac Soc. 2006; 3:424–7. [PubMed: 16799086]
17. Barish GD, Narkar VA, Evans RM. PPAR delta: a dagger in the heart of the metabolic syndrome. J Clin Invest. 2006; 116:590–7. [PubMed: 16511591]
18. Sugii S, et al. PPARgamma activation in adipocytes is sufficient for systemic insulin sensitization. Proc Natl Acad Sci U S A. 2009; 106:22504–9. [PubMed: 20018750]
19. Lefterova MI, et al. Cell-specific determinants of peroxisome proliferator-activated receptor gamma function in adipocytes and macrophages. Mol Cell Biol. 2010; 30:2078–2089. [PubMed: 20176806]
20. He W, et al. Adipose-specific peroxisome proliferator-activated receptor gamma knockout causes insulin resistance in fat and liver but not in muscle. Proc Natl Acad Sci USA. 2003; 100:15712–7. [PubMed: 14660788]
21. Hutley LJ, et al. Fibroblast growth factor 1: a key regulator of human adipogenesis. Diabetes. 2004; 53:3097–106. [PubMed: 15561939]
22. Hutley LJ, et al. A putative role for endogenous FGF-2 in FGF-1 mediated differentiation of human preadipocytes. Mol Cell Endocrinol. 2011; 339:165–71. [PubMed: 21539890]
23. Fon Tacer K, et al. Research resource: Comprehensive expression atlas of the fibroblast growth factor system in adult mouse. Mol Endocrinol. 2010; 24:2050–64. [PubMed: 20667984]
24. Moore DD. Physiology. Sister act. Science. 2007; 316:1436–8. [PubMed: 17556573]
25. Kliewer SA, Mangelsdorf DJ. Fibroblast growth factor 21: from pharmacology to physiology. Am J Clin Nutr. 2010; 91:254S–257S. [PubMed: 19906798]
26. Kharitonenkov A. FGFs and metabolism. Curr Opin Pharmacol. 2009; 9:805–810. [PubMed: 19683963]

References in methods

27. Fang S, et al. Corepressor SMRT promotes oxidative phosphorylation in adipose tissue and protects against diet-induced obesity and insulin resistance. Proc Natl Acad Sci U S A. 2011; 108:3412–3417. [PubMed: 21300871]
28. Hevener AL, et al. Muscle-specific Pparg deletion causes insulin resistance. Nat Med. 2003; 9:1491–1497. [PubMed: 14625542]
29. Nofsinger RR, et al. SMRT repression of nuclear receptors controls the adipog*enic set* point and metabolic homeostasis. Proc Natl Acad Sci U S A. 2008; 105:20021–20026. [PubMed: 19066220]
30. Barish GD, et al. Bcl-6 and NF-Kappa B cistromes medi*ate opposing regulation o*f the innate immune response. Genes Dev. 2010; 15:2760–2765. [PubMed: 21106671]
31. Springer ML, Ip TK, Blau HM. Angiogenesis monitored by perfusion with a space-filling microbead suspension. Mol Ther. 2000; 1:82–87. [PubMed: 10933915]

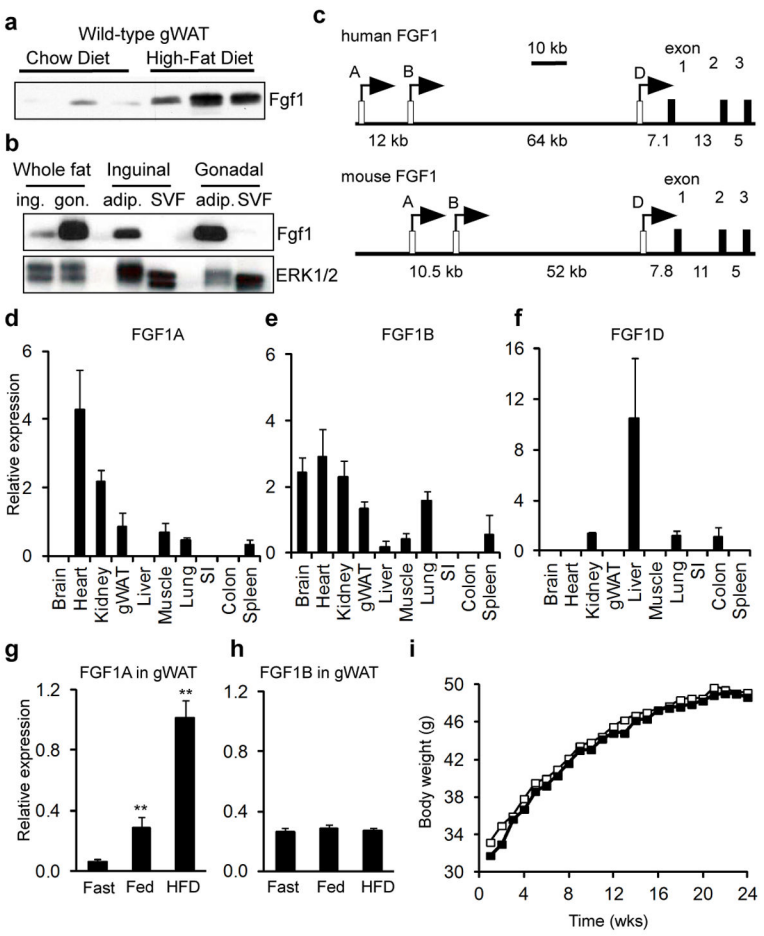

Figure 1. FGF1A is induced in adipose tissue by high-fat diet (HFD)

a, Western blot of FGF1 in gonadal white adipose (gWAT) of chow or HFD-fed wild-type mice (n=3). **b,** Western blot of FGF1 in whole fat, adipocyte (adip.) and stromal vascular fractions (SVF) of inguinal (ing.) and gonadal (gon.) white adipose of chow-fed wild-type mice (ERK1/2 loading control). **c**, Diagram depicting three distinct promoters driving the untranslated exons 1A, 1B, and 1D (open bars) of human and mouse *FGF1* genes. Alternative splicing of untranslated exons results in identical FGF1 polypeptides. **d–f**, mRNA tissue distribution in mice for *FGF1A* (**d**), *FGF1B* (**e**), and *FGF1D* (**f**). **g, h**, mRNA levels of *FGF1A* (**g**) and *FGF1B* (**h**) in gWAT of chow fed, 2-weeks HFD-fed, or overnight fasted wild-type mice (n = 5). **i**, Body weight of HFD-fed wild-type and *FGF1*$^{-/-}$ mice over 24 weeks. Data expressed as mean ± S.D. * *p<0.01.

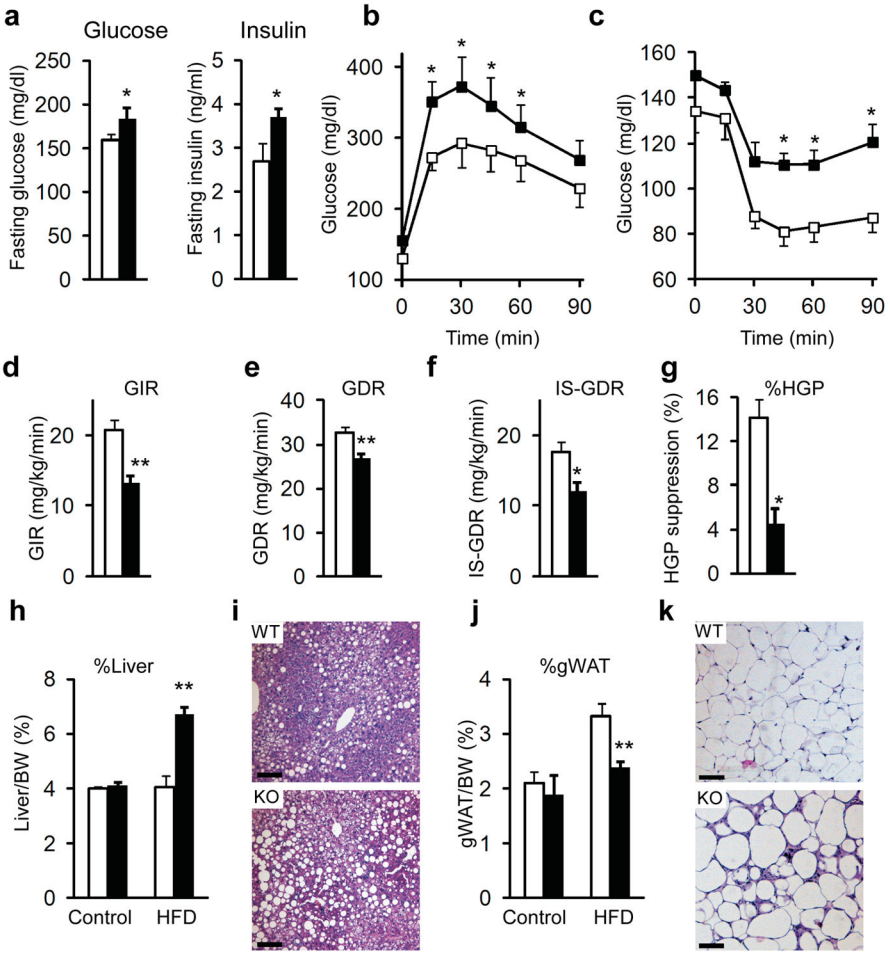

Figure 2. Loss of FGF1 results in diet-induced insulin resistance

Metabolic studies on 24 week old male wild-type (open bars) and *FGF1*$^{-/-}$ (filled bars) mice fed a HFD for 16 weeks. **a**, Fasting serum glucose and insulin levels. **b, c**, Glucose (**b**) and insulin (**c**) tolerance tests. **d–g**, Glucose infusion rate (GIR) (**d**), glucose disposal rate (GDR) (**e**), insulin-stimulated GDR (IS-GDR) (**f**), and percent suppression of hepatic glucose production (HGP) (**g**) during hyperinsulinemic-euglycemic clamp studies. **h**, Liver (percent body weight) from chow and HFD-fed mice (n=6–7). **i**, H&E staining of liver from HFD-fed wild-type (WT) and *FGF1*$^{-/-}$ (KO) mice. **j**, Gonadal white adipose (gWAT) (percent body weight) from chow and HFD-fed mice (n=6–7)**. k**, H&E staining of gWAT from HFD-fed wild-type (WT) and *FGF1*$^{-/-}$ (KO) mice. Scale bar = 100 μm. Data expressed as mean ± S.D. *p<0.05, **p<0.01.

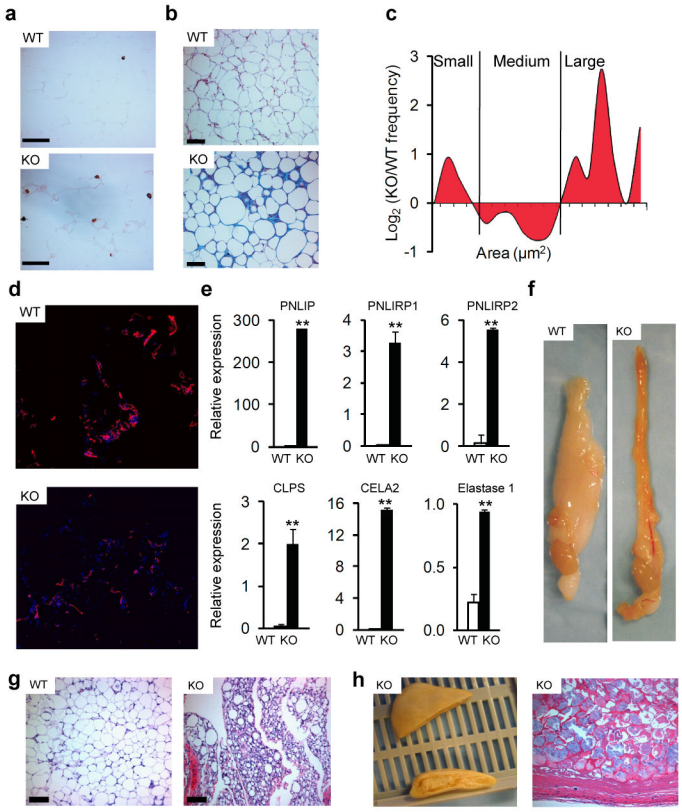

Figure 3. Loss of FGF1 results in defects in adipose remodelling during HFD

a, Immunohistochemistry for the macrophage marker, F4/80 in gWAT from HFD-fed wild-type (WT) and *FGF1*$^{-/-}$ (KO) mice. **b**, Trichrome staining for collagen deposition in gWAT from HFD-fed wild-type (WT) and *FGF1*$^{-/-}$ (KO) mice. **c**, Quantitation of adipose cell cross-sectional area from HFD-fed mice, expressed as the ratio of the number of cells from *FGF1*$^{-/-}$ (KO) to wild-type (WT) mice defined as small (1000–4000 μm^2), medium (4000–10000 μm^2) and large (>10000 μm^2) cells. **d**, Fluorescence microscopy of gWAT from HFD-fed wild-type (WT) and *FGF1*$^{-/-}$ (KO) mice perfused with microbeads (red) and counterstained with DAPI (blue). **e**, QPCR verification of induction of genes associated with fat necrosis in HFD-fed wild-type (open bars) and *FGF1*$^{-/-}$ (closed bars) mice. **f**, gWAT depots from HFD to chow converted (HCC) wild-type (WT) and *FGF1*$^{-/-}$ (KO) mice. **g**, H&E staining of gWAT from HCC wild-type (WT) and *FGF1*$^{-/-}$ (KO) mice. **h**, Image and H&E staining of dissociated necrotic WAT taken from peritoneal cavity of HCC *FGF1*$^{-/-}$ (KO) mice. Scale bar = 100 μm. Data expressed as mean ± S.D. **p<0.01.

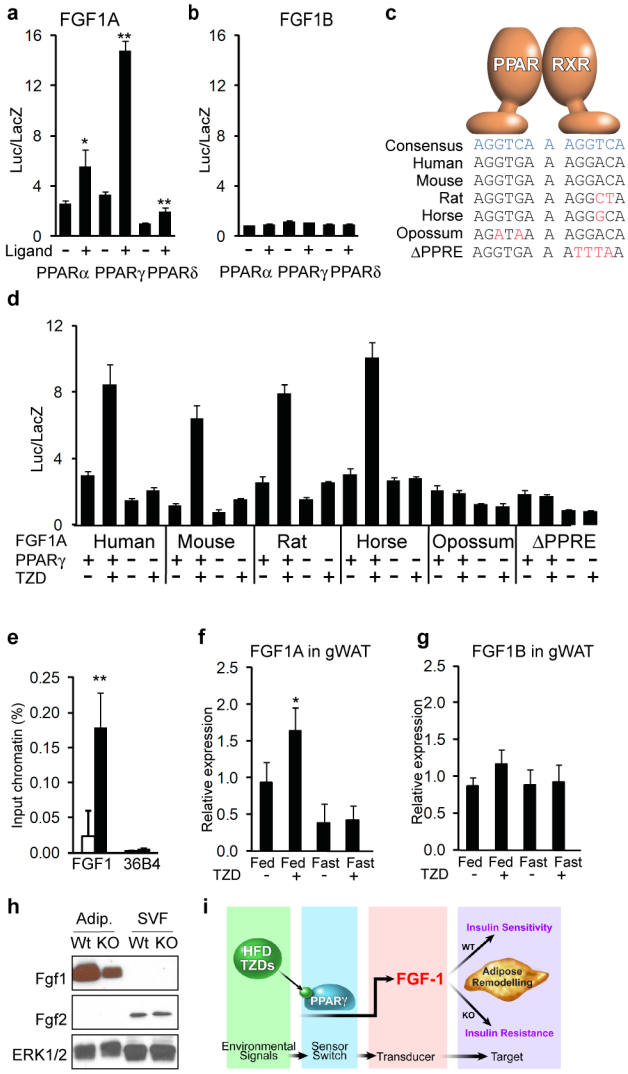

Figure 4. FGF1 is a direct transcriptional target of PPARγ

a, **b**, Luciferase reporter assays of *FGF1A* (**a**) and *FGF1B* (**b**) promoters co-transfected with PPARs +/− ligand. **c**, Sequence alignment of the putative PPRE within the *FGF1A* promoter from different species. Red indicates nucleotide variations between the PPREs relative to human. **d**, Species-specific response of the *FGF1A* promoters to PPARγ +/− ligand using luciferase reporter assays. **e**, Chromatin immuno-precipitation of PPARγ on the *FGF1A* promoter in differentiated 3T3-L1 cells (open bars IgG, closed bars PPARγ antibody). **f, g**, Levels of FGF1A (**f**) *FGF1B* (**g**) mRNA in gonadal white adipose (gWAT) of fed or overnight fasted wild-type mice (n=5) with or w/o TZD (5mg/kg for 3 days i.p). **h**, Western blot of FGF1, FGF2 in adipocyte (adip.) and stromal vascular (SVF) fractions of gonadal white adipose (gWAT) from chow fed wild-type (WT) and *aP2-Cre; PPARγ$^{fl/fl}$* (adipocyte-specific PPARγ knockout) mice (KO) (ERK1/2 loading control). **i**, Model depicting the role of the PPARγ-FGF1 axis in adipose remodelling and insulin sensitivity. Data expressed as mean ± S.D. *p<0.05,**p<0.01.